Saddle-splay modulus of reverse microemulsions: Experimental determination using small-angle neutron scattering and dielectric relaxation spectroscopy

P. M. Geethu,[1] Indresh Yadav,[2] Ethayaraja Mani,[3] Vinod K. Aswal,[2] and Dillip K. Satapathy[1,*]

[1]*Soft Materials Laboratory, Department of Physics, IIT Madras, Chennai 600 036, India*

[2]*Solid State Physics Division, Bhabha Atomic Research Centre, Mumbai 400 085, India*

[3]*Polymer Engineering and Colloids Science Laboratory, Department of Chemical Engineering, IIT Madras, Chennai 600 036, India*

(Received 3 July 2018; published 12 November 2018)

The elastic bending constants κ (elastic bending modulus) and $\bar{\kappa}$ (saddle-splay modulus) are key parameters for understanding the properties of microemulsions (MEs), vesicles, biological membranes, and other self-assembled amphiphilic molecular structures. The determination of κ is rather straight forward, whereas $\bar{\kappa}$ is quiet difficult to access experimentally. Nonetheless, the estimation of $\bar{\kappa}$ is crucial, owing to its importance in governing the intricate phase behavior, topology, and stability of these self-assembled structures. Here, we present an elegant protocol to determine the saddle-splay modulus of the spherical droplet phase of microemulsions using small-angle neutron scattering (SANS) and dielectric relaxation spectroscopy (DRS) techniques. The κ of AOT [sodium 1,4-bis(2-ethylhexoxy)-1,4-dioxobutane-2-sulfonate)]stabilized reverse MEs is estimated by probing their percolation transitions. Further, the effective elastic bending constant K is determined from the polydispersity of ME droplets measured using SANS, where the droplet deformations due to thermal fluctuations are described in terms of spherical harmonics. Strikingly, the ratio $\bar{\kappa}/\kappa$ lies in the acceptable range, $-2 < \bar{\kappa}/\kappa < 0$, for the spherical droplet phase of MEs [R. H. Templer, B. J. Khoo, and J. M. Seddon, Langmuir **14**, 7427 (1998)], which further validates the proposed strategy to estimate the saddle-splay modulus.

DOI: 10.1103/PhysRevE.98.052604

I. INTRODUCTION

Microemulsions (MEs) are colloidal dispersions of water and oil stabilized by surfactant molecules. They exhibit ultralow interfacial tension along with extensive interfacial area between the immiscible liquids. The mesoscale structure, phase behavior, and dynamics of MEs have been widely investigated both from the fundamental research point of view as well as for the manifold technological applications [1–3]. For instance, MEs find potential applications in food technology [4], enhanced oil recovery where the mobilization and solubilization of oil from underground reservoirs is involved [3,5], cleaning technologies [6], cosmetic industry [7], drug delivery [1], the biomedical field [2], and nanoparticle synthesis [8].

MEs form a rich variety of microstructures ranging from droplets (oil in water or water in oil) to lamellar and bicontinuous phases [9]. It is known that the range of microstructures is mostly related to the spontaneous curvature c_0 of the self-assembled surfactant monolayer and its deformations. Indeed, the dominant soft modes associated with the surfactant monolayer are curvature deformations, since the thermal energy is sufficient to induce bending of the surfactant film but cannot cause stretching. By considering an analogy with liquid crystals, Helfrich has introduced the elastic curvature energy F_c of the self-assembled surfactant layer, given by [10]

$$F_c = \int dA\left[\frac{\kappa}{2}(c_1 + c_2 - 2c_0)^2 + \bar{\kappa}(c_1 c_2)\right], \qquad (1)$$

where c_1 and c_2 are the two principal curvatures, such that their arithmetic sum constitutes the mean curvature and their product gives the Gaussian curvature. Further, the elastic constants κ (elastic bending modulus or elastic bending rigidity) and $\bar{\kappa}$ (saddle-splay modulus) are related to the deviations to the mean curvature and Gaussian curvature, respectively. The elastic bending modulus κ represents the energy required to bend a unit area of the surfactant monolayer by a unit amount and is always positive ($\kappa > 0$). A plethora of techniques such as ellipsometry [11], dielectric relaxation spectroscopy [12,13], Kerr effect measurements [14,15], and small-angle x-ray and neutron scattering [13,16] have been employed to determine the κ of microemulsions.

The role of the saddle-splay modulus $\bar{\kappa}$ in governing the curvature deformations is highly significant while considering the topological reformations and phase transitions in microemulsions [17]. $\bar{\kappa}$ can be either positive or negative. Negative values of $\bar{\kappa}$ indicate spherical and lamellar structures, whereas positive values correspond to saddle-shaped surfactant film (e.g., the sponge phase in microemulsions). It is important to note that during a first-order phase transition from lamellar to sponge-like phases, which can be achieved by an increase in temperature for nonionic surfactant systems and by changing the salinity for ionic surfactant systems, the sign of $\bar{\kappa}$ switches from negative to positive [18]. Besides, the

*dks@iitm.ac.in

swollen lamellae stabilized by thermal undulations which will not undergo phase transition to sponge-like structures are also probable [19]. Consequently, the measurement of $\bar{\kappa}$ is vital to unravelling the structural transitions occurring in MEs in the presence of external stimuli.

Further, $\bar{\kappa}$ represents the energy change associated with the deviations in Gaussian curvature c_1c_2 as indicated by Eq. (1). According to the Gauss-Bonnet theorem, the surface integral of Gaussian curvature is invariant under deformations which do not involve any topological transformations, indicating that obtaining an experimental signal sensitive to $\bar{\kappa}$ [20] is quite difficult. Although few reports present the determination of $\bar{\kappa}$ for MEs using neutron spin echo spectroscopy [21–23], the direct evaluation of $\bar{\kappa}$ is highly challenging since it is related to the change in energy during the topological reformations, which are difficult to manipulate, both in experiments as well as in simulations [20]. Moreover, neutron spin echo spectroscopy, being the highest energy resolution neutron scattering technique, is not readily accessible worldwide and is also cumbersome.

Here, we present a strategy to determine the saddle-splay modulus $\bar{\kappa}$ of the spherical droplet phase of microemulsions from the measured values of the effective elastic bending constant K and the elastic bending modulus κ, using small-angle neutron scattering (SANS) and dielectric relaxation spectroscopy (DRS) techniques. The effective elastic bending constant K ($K = 2\kappa + \bar{\kappa}$) is estimated from the polydispersity of ME droplets obtained using SANS, by following a method which was previously considered for oil-in-water microemulsions stabilized with nonionic surfactants [24]. Here, the thermal fluctuations of microemulsion droplets are described by using spherical harmonics [24]. Next, the elastic bending modulus κ of the surfactant monolayer is independently determined by probing the temperature-dependent percolation transition in MEs [12,25]. Finally, the saddle-splay modulus $\bar{\kappa}$ is evaluated from the knowledge of K and κ and is compared with the literature results. The widely studied, model, water-in-oil microemulsions stabilized by AOT [sodium 1,4-bis(2-ethylhexoxy)-1,4-dioxobutane-2-sulfonate] surfactant are chosen for the present investigation.

The paper is organized as follows. Section II discusses the theoretical formalisms required to estimate the effective elastic bending constant K and the elastic bending modulus κ of microemulsions. Next, in Sec. III, the details of the experiments are briefly described. Finally, Sec. IV discusses (i) the determination of effective elastic bending constant K from the polydispersity of droplets, (ii) the estimation of elastic bending modulus κ from the percolation transition temperature T_P and the core radius R of microemulsion droplets, and (iii) the evaluation of saddle-splay modulus $\bar{\kappa}$ from K and κ.

II. THEORETICAL FRAMEWORK

The saddle-splay modulus $\bar{\kappa}$ of the spherical droplet phase of microemulsions is evaluated from the effective elastic bending constant K and the elastic bending modulus κ by using the formula $\bar{\kappa} = K - 2\kappa$. The theoretical formalisms followed in the present study to estimate K and κ of MEs are discussed in Secs. II A and II B.

A. Estimation of effective elastic bending constant K from the polydispersity of microemulsion droplets

The structure and phase behavior of microemulsions are mostly governed by a subtle competition between the curvature elasticity and the entropy of the system. Here, the interfacial tension between the dispersed phase and the solvent phase is considered as negligible [24,26]. Consequently, the free energy F of microemulsions can be written in terms of the curvature energy F_c and the mixing entropy F_{ent}, given as [10]

$$F = F_c + F_{\text{ent}} = \int dA\left[\frac{\kappa}{2}(c_1+c_2-2c_0)^2+\bar{\kappa}(c_1c_2)\right]+Nk_BTf(\phi). \quad (2)$$

Here, the entropy of mixing term $f(\phi)$ for microemulsion droplets having a volume fraction ϕ can be obtained from the random-mixing approximation proposed by Milner and Safran [27], given by

$$f(\phi) = (1/\phi)\{\phi\ln\phi + (1-\phi)\ln(1-\phi)\}. \quad (3)$$

Further, for the case of spherical droplets of radius R, the free energy per unit area can be written from Eq. (2) as

$$f = 2\kappa\left(\frac{1}{R}-\frac{1}{R_0}\right)^2 + \frac{\bar{\kappa}}{R^2} + \frac{k_BT}{4\pi R^2}f(\phi). \quad (4)$$

When the droplet phase of microemulsions is in equilibrium with the excess phase of the solubilizate, the droplets achieve maximum size R_m such that any further addition of the solubilizate will lead to emulsification failure. Further, a relation connecting the maximum droplet size R_m (or equilibrium droplet size), the spontaneous radius R_0, and the elastic bending constants κ and $\bar{\kappa}$ can be obtained from the minimization of the free energy equation (4) and is given as

$$\frac{R_m}{R_0} = \frac{2\kappa+\bar{\kappa}}{2\kappa} + \frac{k_BT}{8\pi\kappa}f(\phi). \quad (5)$$

At equilibrium, microemulsion droplets collide and exchange surfactant and fluid with each other, causing distortions in droplet size and shape. According to Safran, the thermally induced droplet deformations can be described by using spherical harmonics $Y_{lm}(\theta,\phi)$ [24,28,29],

$$R(\theta,\phi) = R_m\left[1+\sum_{l,m}u_{l,m}Y_{l,m}(\theta,\phi)\right], \quad (6)$$

where θ and ϕ represent the spherical polar coordinates. Further, it is shown that the major contributions toward droplet deformations arise from the first two harmonics of $Y_{lm}(\theta,\phi)$, i.e., $l = 0$ and $l = 2$, which represent the size fluctuations and shape fluctuations of ME droplets, respectively [24]. The mean-square amplitude of size fluctuations (corresponding to $l = 0$) of droplets is given by [24]

$$\langle|u_0|^2\rangle = \frac{k_BT}{6(2\kappa+\bar{\kappa})-8\kappa(R/R_0)+(3k_BT/2\pi)f(\phi)}. \quad (7)$$

It is important to note here that the droplet deformations described by $\langle|u_{l,m}|^2\rangle$ represent the droplet polydispersity p,

which is given as

$$p^2 = \frac{\langle (R - R_m)^2 \rangle}{R_m^2} \simeq \frac{\langle |u_0|^2 \rangle}{4\pi}. \tag{8}$$

The contributions of higher order terms of $\langle |u_{l,m}|^2 \rangle$ toward polydispersity are negligible and not considered here [24]. Consequently, by substituting Eq. (5) in Eq. (7), the polydispersity index p can be obtained as

$$p^2 = \frac{\langle |u_0|^2 \rangle}{4\pi} = \frac{k_B T}{8\pi(2\kappa + \bar{\kappa}) + 2k_B T f(\phi)}. \tag{9}$$

Here, $2\kappa + \bar{\kappa} = K$ is the effective elastic bending constant of microemulsion droplets. Therefore, by evaluating the polydispersity index p of microemulsion droplets, K can be estimated by using the equation

$$K = \frac{1}{8\pi}\left\{\frac{k_B T}{p^2} - 2k_B T f(\phi)\right\}. \tag{10}$$

B. Percolation transition temperature and determination of elastic bending modulus κ of microemulsions

Several methods have been proposed to estimate the elastic bending modulus κ of the interfacial surfactant monolayer in MEs [11,21,30]. In the present study, κ is obtained by probing the temperature-dependent percolation transition in MEs and the formalism is discussed in this section [12,13].

Microemulsions, formed by the spontaneous self-assembly of surfactant molecules at the water-oil interface, are highly sensitive to thermal fluctuations. By measuring the effect of temperature on structure and phase behavior of MEs, it is possible to estimate the elastic bending modulus κ of the surfactant monolayer at the water-oil interface. De Gennes and Taupin have developed a formalism [31] to determine the persistence length ξ_p of a two-dimensional membrane, which constitutes a fluctuating random interface, by considering the contribution of curvature energy toward the free energy of the system. According to this formalism, ξ_p of a random interface having negligible spontaneous curvature is defined as the length scale over which the angular correlations between two points at the interface decay to zero (or strictly speaking, $1/e$) and is written as

$$\xi_p = a \exp\left(\frac{2\pi\kappa}{k_B T}\right), \tag{11}$$

where a is the lower cutoff in the wavelength of the undulations which is related to the size of the surfactant molecule and κ is the elastic bending modulus of the interfacial surfactant monolayer. Equation (11) signifies that the persistence length of the surfactant layer and its elastic bending modulus are modified with thermal fluctuations. Further, this formalism was extended to elucidate the temperature-dependent phase behavior of microemulsions by Meier [25], where the interfacial surfactant monolayer constitutes the fluctuating random interface. In the context of microemulsions, Meier [25] defined ξ_p as the upper-bound value of the ME droplet radius over which the interfacial surfactant layer remains constantly curved. Accordingly, for MEs with droplet radius $R < \xi_p$, the structure will be spherical and when $R > \xi_p$, it will be deformed.

Microemulsions are known to exhibit temperature-dependent percolation transitions, where the droplets form dynamic clusters with increase in temperature owing to the attractive interaction between the droplets. Electrical conductivity measurements have been widely used to probe the phase behavior of microemulsions. A monumental increase in electrical conductivity is observed with enhancement in temperature and is described using the model of hopping of charge carriers and/or exchange of the droplet contents during percolation transition. At percolation, although the droplet structure remains intact, the shape-restoring interfacial forces are considered to be weak [32]. The percolation transition in microemulsions is characterized by a threshold temperature T_P, which is identified as the temperature at which the gradient of electrical conductivity with respect to temperature shows a maximum. Further, Meier [25] made the assumption that the persistence length of the interfacial surfactant layer should match with the droplet radius R at T_P. Therefore, Eq. (11) can be written as

$$R = a \exp\left(\frac{2\pi\kappa}{k_B T_P}\right). \tag{12}$$

Here, negligible spontaneous curvature of interfacial surfactant monolayer is assumed [33,34]. Using this relation, the elastic bending modulus of the surfactant monolayer can be estimated by measuring the percolation threshold temperature T_P of MEs with different droplet radii [12,13].

III. EXPERIMENTS

A. Sample preparation

Microemulsions were prepared by mixing appropriate amounts of AOT surfactant (99% purity, purchased from Sigma Aldrich), n-decane (99% purity, purchased from Alfa Aesar), and water (Millipore Direct-Q3 ultrapure water system, $\sigma = 5.5 \times 10^{-8}$ S/cm) and shaken well for several minutes using a vortex shaker until the mixture became homogeneous and optically clear. For all the SANS measurements, H_2O was replaced with D_2O (99.9% purity, purchased from Sigma Aldrich) to obtain better contrast. Microemulsion with $W = 33$ and $\phi = 0.1$ was prepared under two different contrast conditions for SANS measurements: (i) core contrast (DHH, D_2O+AOT+n-decane) and (ii) shell contrast (DHD, D_2O+AOT+ deuterated n-decane-d_{22}). To achieve shell contrast (DHD) of MEs, deuterated n-decane-d_{22} purchased from Armar Isotopes, Switzerland (99.9% purity) was used without further purification. The composition of microemulsions is characterized by the parameters W and ϕ, where W denotes the molar ratio of water to surfactant, $W = \frac{n[H_2O]}{n[AOT]}$ and ϕ the volume fraction of droplets, $\phi = \frac{V_{droplets}}{V_{total}} = \frac{V_{water} + V_{AOT}}{V_{water} + V_{AOT} + V_{n-decane}}$. In the present study, AOT-stabilized microemulsions with W ranging from 15 to 40 were prepared. The volume fraction of droplets is $\phi = 0.1, 0.3$.

B. Small-angle neutron scattering

Small-angle neutron scattering (SANS) is used to determine the shape, size, and polydispersity (size distribution) of microemulsion droplets [16,35]. SANS gives the scattering profile, i.e., the coherent differential scattering cross section per unit volume ($d\Sigma/d\Omega$) as a function of scattering vector Q in Fourier space, and the real-space information of the sample (structure and interaction) is extracted by fitting the profiles with suitable mathematical models. For a collection of identical interacting particles (microemulsion droplets), the general equation which describes the scattering data is given as [36]

$$\frac{d\Sigma}{d\Omega}(Q) = nP(Q)S(Q) + B, \tag{13}$$

where n is the number density of microemulsion droplets and is given as $n = \phi/V$, V is the volume of individual ME droplets, and ϕ is their volume fraction. $P(Q)$ is the intraparticle structure factor which gives information about particle shape and size. $S(Q)$ is the interparticle structure factor which describes the spatial distribution of particles and the interaction between them. For noninteracting dilute systems $S(Q)$ is unity. The constant term B accounts for the incoherent scattering background. The intraparticle structure factor $P(Q)$ is given as the square of the single-particle form factor $F(Q)$,

$$P(Q) = \langle |F(Q)|^2 \rangle. \tag{14}$$

For spherical particles of radius R, $F(Q)$ is given as

$$F(Q) = V(\rho_p - \rho_s)\frac{3\{\sin(QR) - QR\cos(QR)\}}{(QR)^3}, \tag{15}$$

where ρ_p and ρ_s are the scattering length densities of particle (ME droplet) and solvent respectively. When the scatterers are spherical core-shell particles having core radius R and shell thickness d, the $F(Q)$ is given as

$$F(Q) = V_1\Delta\rho_{cs}\frac{3\{\sin(QR) - QR\cos(QR)\}}{(QR)^3} + V_2\Delta\rho_{sm}\frac{3\{\sin(QR_d) - QR_d\cos(QR_d)\}}{(QR_d)^3}, \tag{16}$$

where $R_d = R + d$ gives the droplet radius, V_1 and V_2 are the volume of core and droplet (core + shell), and $\Delta\rho_{cs}$ and $\Delta\rho_{sm}$ represent the difference in scattering length density between core and shell and that between shell and matrix respectively. The experimental scattering data are fitted with different theoretical models by following the nonlinear least-squares method. The polydispersity of microemulsion droplets is taken into account by averaging the scattered intensity by a log-normal distribution function. In the present study the SANS profiles are fitted by assuming $S(Q) \sim 1$ [13,37].

SANS measurements were performed in the wave vector transfer [$Q = 4\pi \sin(\theta/2)/\lambda$, where θ is the scattering angle] Q range of 0.017–0.35 Å^{-1} using the SANS-I instrument at the Dhruva reactor, Bhabha Atomic Research Centre, Mumbai, India [38]. The mean wavelength λ of the monochromatic neutron beam was 5.2 Å with a nominal spread ($\Delta\lambda/\lambda$) of 15%. Microemulsion samples were held in HELLMA quartz cells having thicknesses of 2 mm. The scattered neutrons were detected using a linear ^{3}He-based, one-dimensional, position-sensitive neutron detector. The raw data were corrected for electronic background and empty cell scattering and normalized to absolute cross-sectional units using standard procedure. For all the SANS measurements, the temperature of the samples was kept constant at 30 °C. SASFIT software [39] was used for fitting the measured scattering profiles.

C. Dielectric relaxation spectroscopy

The percolation threshold temperatures T_P of microemulsions are precisely determined from conductivity and permittivity measurements performed using dielectric relaxation spectroscopy (DRS). It measures the complex impedance $Z^*(\omega)$ of the sample as a function of frequency, from which the complex dielectric permittivity $\varepsilon^*(\omega)$ is derived using the relation [40]

$$\varepsilon^*(\omega) = \varepsilon'(\omega) - i\varepsilon''(\omega) = \frac{-i}{\omega Z^*(\omega)C_0}, \tag{17}$$

where C_0 is the empty cell capacitance, ω is the angular frequency, and ε' and ε'' are the real and imaginary parts of the complex dielectric permittivity. The complex conductivity $\sigma^*(\omega)$ of the sample is related to the complex dielectric function $\varepsilon^*(\omega)$ as

$$\sigma^*(\omega) = i\omega\varepsilon_0\varepsilon^*(\omega), \tag{18}$$

where ε_0 is the dielectric permittivity of vacuum.

The dielectric measurements were performed at different temperatures starting from 5 °C up to 60 °C in a frequency range 1 Hz to 10 MHz using a high-resolution Alpha dielectric analyzer (Novocontrol, Germany) with active sample cell ZGS as the test interface. A liquid sample cell supplied by Novocontrol (BDS 1308) with a diameter of 20 mm and thickness of 100 μm (obtained using silica spacers) was used in the measurements. Novocontrol Quatro Cryosystem with a temperature stability of 0.1 K is employed for temperature control, where nitrogen gas is used as the heating agent.

IV. RESULTS AND DISCUSSION

The elastic bending constants K and κ of AOT-stabilized reverse microemulsions are determined by following the formalisms described in Secs. II A and II B. Further, the saddle-splay modulus $\bar{\kappa}$ is deduced from K and κ. Its comparison with the values reported in the literature is also presented. Here, we would like to mention that the proposed strategy to estimate $\bar{\kappa}$ is demonstrated by considering a stable composition of water-AOT-n-decane reverse microemulsion with $W = 33$ and $\phi = 0.1$, and can be further verified for other compositions and other microemulsions as well.

A. Estimation of K from the polydispersity of ME droplets

To estimate the effective elastic bending constant K of AOT-stabilized reverse microemulsions using the formalism described in Sec. II A, the polydispersity of ME droplets is determined from small-angle neutron scattering experiments. Two different contrast conditions given as the core (DHH) contrast and the shell (DHD) contrast of microemulsions are

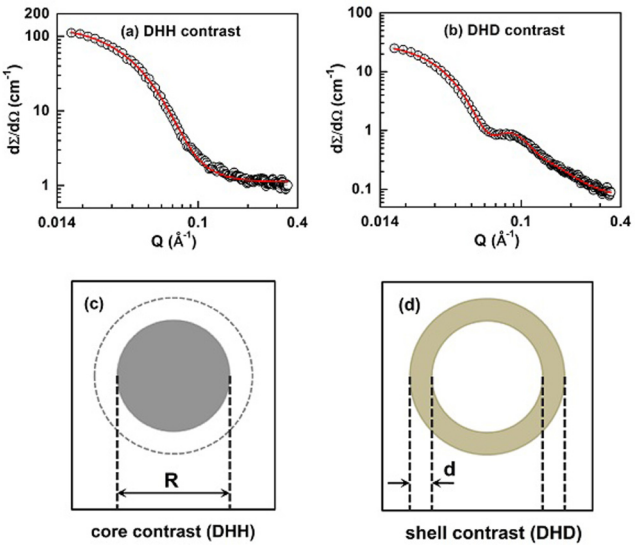

FIG. 1. SANS profiles together with the fit functions for AOT-stabilized reverse microemulsions with $W = 33$ and $\phi = 0.1$ in two different contrast conditions given as (a) core contrast (DHH) and (b) shell contrast (DHD). The schematic representation of microemulsions in DHH and DHD contrast conditions are shown in (c) and (d).

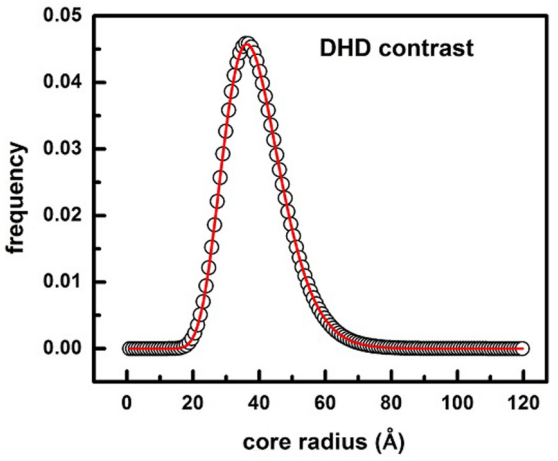

FIG. 2. Size distribution of microemulsion droplets in shell (DHD) contrast together with the fit to Eq. (19) where the fitting parameters are given by the mean droplet radius $R_0 = 45.2 \pm 0.5$ Å and the effective elastic bending constant of surfactant monolayer $K = 0.42 \pm 0.02\, k_B T$.

employed in SANS measurements for the precise determination of the structural parameters of ME droplets. SANS profiles together with best fits to the theoretical models for microemulsions with W=33 and ϕ=0.1, in DHH and DHD contrast conditions are shown in Figs. 1(a) and 1(b), respectively. Further, the schematic representation of microemulsions in DHH and DHD contrast are, respectively, shown in Figs. 1(c) and 1(d). In DHH contrast, H_2O was replaced with D_2O such that the scattering is mostly dominated by the D_2O core of the ME droplet. Accordingly, the form factor for spherical droplets given by Eq. (15) is used to model the SANS profile. The core radius R and the polydispersity of droplets obtained from the best fit of the SANS profile are given as 45.0 ± 0.3 Å and 0.29 ± 0.02 respectively. Further, SANS measurements have been performed on microemulsions in shell (DHD) contrast condition. The high contrast between the surfactant shell and the other components of the microemulsion permits a detailed fitting of polydispersity of ME droplets as well as an accurate determination of their size distribution. Here, the microemulsions are prepared with deuterated water (D_2O) and oil (n-decane-d_{22}) and hydrogenated surfactant, such that the scattering is nearly exclusively from the surfactant shell. Consequently, the scattering profile is modeled with a spherical core-shell form factor given by Eq. (16). The mean value of core radius R, shell thickness d, and polydispersity of droplets calculated from the best fit of SANS profile are given as 46.1 ± 0.3 Å, 11.6 ± 0.7 Å and 0.23 ± 0.01, respectively. Here, the best fit to the scattering profiles, with reasonable values for core radii and AOT shell thickness, was obtained when a log-normal distribution of droplet sizes was assumed. Having unambiguously determined the polydispersity of ME droplets from SANS measurements, next the effective bending constant K is evaluated using Eq. (10). By substituting $p = 0.23$ in Eq. (10), the effective elastic bending constant K is obtained as $K = 0.97 \pm 0.03\, k_B T$, which is reasonably close to the values reported in the literature for microemulsions [24,41].

It is important to mention that there are mainly two effects which contribute to the polydispersity of microemulsion droplets: (i) The radii of ME droplets are distributed around a mean droplet radius R and are mostly determined by the interfacial tension at the water-oil interface in the presence of a surfactant. (ii) The surfactant shell of a ME droplet undergoes constant thermal shape fluctuations due to the floppiness of the shell. Accordingly, it can be inferred that the size distribution or polydispersity emanate due to the form fluctuations of ME droplets which strongly depend on the elastic bending constants of the interfacial surfactant monolayer. An interesting investigation by Jung *et al.* [42] on the self-assembly of surfactants to form unilamellar vesicles presents a strategy to estimate the effective elastic bending constant K (where $K = 2\kappa + \bar{\kappa}$) of surfactant bilayer from the size distribution of vesicles. This formalism is derived based on the assumption that the equilibrium size distribution of an ensemble of vesicles is governed by the balance between the entropy of mixing and the curvature energy of the surfactant bilayers [42,43]. Microemulsions in droplet phase have a close resemblance to vesicles in many ways. The properties of both microemulsions and vesicles are mostly governed by the curvature elasticity of self-assembled surfactant layer and the configurational entropy of the system. Consequently, the above formalism can be applied to microemulsions as well. According to this formalism, the size distribution of ME droplets is obtained as

$$C_N = \left\{ C_M \exp\left[\frac{-4\pi K}{k_B T} \left(1 - \frac{R_0}{R} \right)^2 \right] \right\}^{\frac{R^2}{R_0^2}}, \qquad (19)$$

where C_M and C_N are the molar fractions of microemulsion droplets having surfactant aggregation number M and N respectively ($C_M = X_M/M$ and $C_N = X_N/N$). Also, the

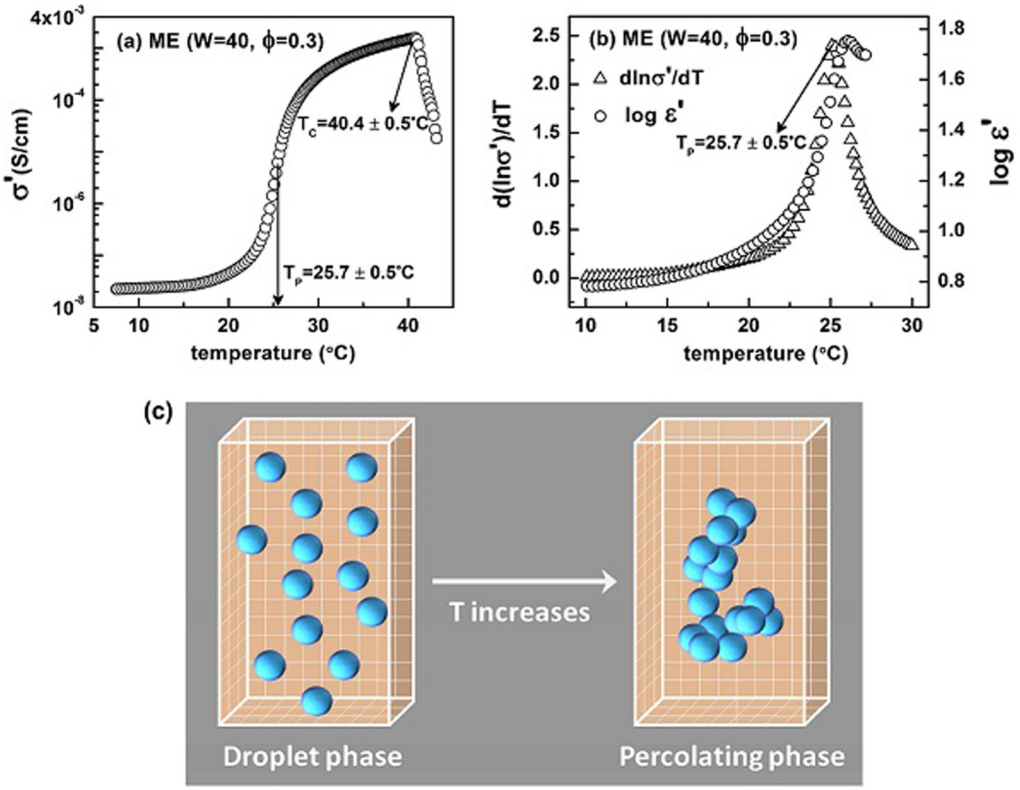

FIG. 3. Determination of percolation threshold temperature T_P of microemulsions from temperature dependence of electrical conductivity and dielectric permittivity. (a) Electrical conductivity σ' measured as a function of temperature for AOT-stabilized reverse microemulsion. The percolation threshold temperature $T_P \sim 25.7 \pm 0.5\,^{\circ}$C and the critical temperature of phase separation $T_C \sim 40.4 \pm 0.5\,^{\circ}$C are shown. (b) The first derivative of logarithmic conductivity with respect to temperature ($d \ln \sigma'/dT$) and the real part of complex dielectric permittivity ϵ' as a function of temperature are given. The peak in ϵ' almost coincides with the maximum of $d \ln \sigma'/dT$, which also marks the percolation threshold T_P. All the measurements are performed at an applied frequency of 10^4 Hz for microemulsion with $W = 40$ and $\phi = 0.3$. (c) The schematic representation of temperature-dependent percolation transition in reverse microemulsions, where the dynamic droplet cluster formation during percolation is shown.

aggregation number M and N are given as $M = 4\pi R_0^2/A_0$ and $N = 4\pi R^2/A_0$, where A_0 is the average molecular area of surfactant. Further Eq. (19) implies that the broadness of size distribution of ME droplets is mostly determined by the effective bending constant K. In other words, for smaller values of K, the surfactant monolayer is more sensitive to thermal fluctuations, indicating a broader size distribution of ME droplets. Accordingly, the effective elastic bending constant K of the surfactant monolayer of MEs, which includes the elastic bending modulus κ and saddle-splay modulus $\bar{\kappa}$, can be determined from the size distribution of ME droplets. The size distribution of microemulsion droplets obtained from the scattering profile is shown in Fig. 2 and is fitted to Eq. (19) to determine the effective elastic bending constant K. The best fit to Eq. (19) gives $K = 0.42 \pm 0.02\, k_B T$ and the mean droplet radius $R_0 = 45.2 \pm 0.5$ Å.

It has to be noted that when the contribution of configurational entropy toward K is excluded in the calculations discussed in Sec. II A, the values obtained for K in both methods are almost comparable. Further, a classic approach by Morse and Milner [44] has shown that the free energy of a vesicle increases logarithmically with vesicle size, which arises from the loss of entropy due to the absence of undulation modes of wavelength larger than the size of the vesicle. In other words, the contribution of thermal undulations of a vesicle toward the free energy increases with vesicle size and it inhibits the formation of larger vesicles. According to them, the size distribution of vesicles, in the limit where the radius approaches the thickness of the surrounding membrane, is given as

$$\rho_v(n) \propto n^{-\alpha_v} \exp\left(\frac{-n}{n_\mu}\right) \exp\left(\frac{-n_c}{n}\right), \tag{20}$$

where $\rho_v(n)$ is the number density of vesicles that contain n surfactant molecules, n_μ represents a vesicle size characteristic of the exponential decay of $\rho_v(n)$, n_c is the cutoff size when the vesicle radius o approaches the thickness of the surfactant layer and α_v is a positive coefficient given as $\alpha_v = 7/6$. Further, the self-assembled microemulsions have close resemblance to vesicles, and the function given by Eq. (20) produces a reasonable fit to the measured size distribution of microemulsion droplets with a sharp peak near the lower cutoff size n_c. Indeed, the suitability of Eq. (20) to reasonably fit the measured size distribution of microemulsions indicates that the above formalism [Eq. (20)] is also appropriate for

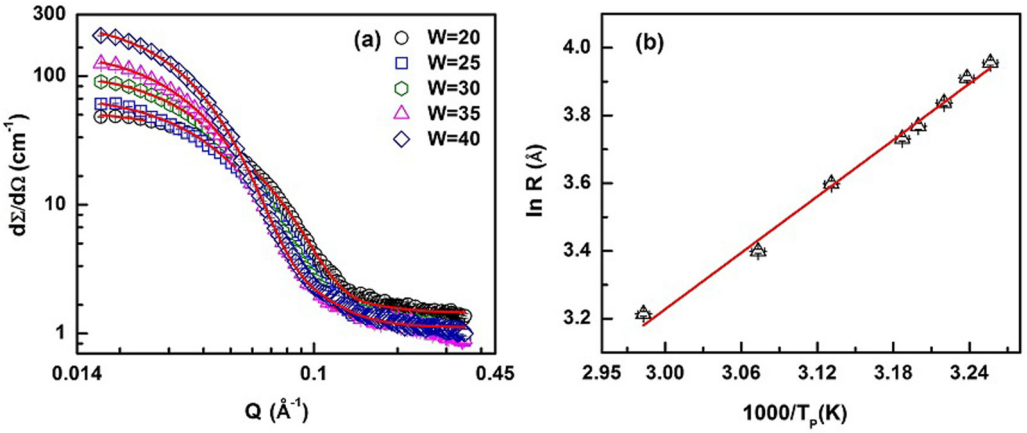

FIG. 4. (a) Measured SANS profiles together with the fits for AOT-stabilized reverse microemulsions with molar ratio of water to surfactant $W = 20$, 25, 30, 35, and 40. The volume fraction of droplets is kept constant at $\phi = 0.1$. (b) Droplet core radius in logarithmic scale as a function of inverse of percolation threshold temperature T_P for microemulsions with different water to surfactant ratio ranging from $W = 15$ to $W = 40$ and volume fraction of droplets $\phi = 0.1$. The straight line shows the fit according to Eq. (12).

microemulsions, where the droplet size of MEs is comparable to the surfactant shell thickness.

B. Percolation dynamics in MEs and estimation of κ from T_P

A well-established approach to estimating the elastic bending modulus κ of microemulsions is by determining the percolation transition temperature T_P for a set of MEs having different core radii R, with fixed number density (volume fraction) of droplets, as discussed in Sec. II B [12,16,25]. Here, the T_P of reverse microemulsions is precisely determined from conductivity as well as from dielectric permittivity measurements. The variation of electrical conductivity σ' as a function of temperature measured at 10^4 Hz for the microemulsion with $W = 40$ and $\phi = 0.3$ are shown in Fig. 3(a). From the temperature-dependent conductivity spectra, T_P is evaluated as the inflection point at which the conductivity gradient shows a maximum [45,46]. Further, the temperature-dependent variation of dielectric permittivity ϵ' and the first derivative of conductivity with respect to temperature ($d \ln \sigma'/dT$) are shown in Fig. 3(b). The percolation temperature is identified as the local maximum of dielectric permittivity which nearly coincides the peak in conductivity gradient. Consequently, the percolation temperature and the critical temperature of phase separation are calculated as $T_P \sim 25.7 \pm 0.5\,^{\circ}\mathrm{C}$ and $T_C \sim 40.4 \pm 0.5\,^{\circ}\mathrm{C}$, respectively, for microemulsion with $W = 40$ and $\phi = 0.3$. Hereby, the unambiguous determination of T_P from conductivity as well as permittivity measurements is illustrated. The schematic representation of dynamic droplet cluster formation during percolation transition, which constitutes the significant increase in conductivity for a small change in temperature, is shown in Fig. 3(c).

Next, the determination of core radius of ME droplets from SANS measurements is discussed. The scattering profiles together with the fitted models for microemulsions in core contrast condition (D_2O + AOT + n-decane − DHH) with $W = 20$, 25, 30, 35, 40 and $\phi = 0.1$ are shown in Fig. 4(a). Here, H_2O is replaced with D_2O in order to obtain better scattering length density contrast $(\rho_{D_2O} - \rho_{\text{n-decane}})^2$ mostly from the water core of microemulsion droplets. The measured scattering profiles are modeled with a form factor for spherical particles as discussed in Sec. II B. While modeling the data, the scattering from the AOT surfactant shell is not taken into account owing to their negligible contrast $(\rho_{\text{AOT}} - \rho_{\text{n-decane}})^2$. The core radius and polydispersity of droplets obtained from the best fit of SANS profiles are given in Table I.

Having estimated the percolation temperature T_P and core radius R, the elastic bending modulus of interfacial AOT surfactant monolayer is determined by following the formalism discussed in Sec. II B. The logarithmically scaled droplet radius R is plotted against the inverse of percolation temperature T_P and is shown in Fig. 4(b). The linear dependencies of the quantities predicted by Eq. (12) can be seen from Fig. 4(b). From the slope, the elastic bending modulus of microemulsion is obtained as $\kappa = 1.46 \pm 0.04\, k_B T$.

Following the same method, Meier estimated the elastic bending modulus of AOT-stabilized microemulsions with hexane and iso-octane as oil phase and found $\kappa = 0.9\, k_B T$ and $\kappa = 1\, k_B T$, respectively [25]. Nagao *et al.* [47] determined the bending modulus for water-AOT-n-decane microemulsions to be $\sim 1.4\, k_B T$ by measuring the fluctuations of surfactant shell using neutron spin echo spectroscopy. Further, Binks *et al.*

TABLE I. Core radius R and polydispersity of spherical droplets of microemulsions with water to surfactant molar ratio $W = 20$, 25, 30, 35, and 40, obtained from the best fit to the SANS profiles shown in Fig. 4. The volume fraction of droplets is kept fixed at $\phi = 0.1$.

Molar ratio of water to surfactant (W)	Mean droplet radius R (Å)	Polydispersity index
20	31.9 ± 0.2	0.28 ± 0.03
25	35.1 ± 0.2	0.28 ± 0.03
30	41.4 ± 0.3	0.29 ± 0.03
35	46.8 ± 0.3	0.29 ± 0.04
40	53.1 ± 0.4	0.30 ± 0.04

[11] measured the elastic bending modulus of interfacial surfactant monolayer in MEs by using ellipsometry and reported the value of $\kappa = 1.1\,k_BT$. Kellay *et al.* [48] carried out a thorough investigation to establish the correlation between the properties of surfactant monolayers and the phase behavior of microemulsions and found the value of κ for water-AOT-n-decane reverse microemulsions to be nearly equal to $1\,k_BT$. All these findings are also inline with the value of κ obtained for the microemulsions following the procedure described in Sec. II B.

Further, we would like to mention that, in this work, the droplet radius is measured at ambient temperature ($T = 30\,^{\circ}$C) assuming that the change in droplet size below T_P is small. Indeed in our previous work, we estimated the error involved in neglecting the temperature dependence of core radius R while determining the elastic bending modulus κ and found it to be negligible [13].

C. Evaluation of $\bar{\kappa}$ from K and κ

From the estimated values of effective bending constant K and elastic bending modulus κ, the saddle-splay modulus $\bar{\kappa}$ is calculated using the formula $\bar{\kappa} = K - 2\kappa$. For AOT-stabilized reverse microemulsions, the saddle-splay modulus is obtained as $\bar{\kappa} \sim -1.95 \pm 0.11\,k_BT$. The negative value of $\bar{\kappa}$ is expected for spherical droplets. The saddle-splay modulus being correlated to the topology of the droplet surface, governs the size fluctuations of ME droplets, and thus contributes to the polydispersity of droplets. In particular, $\bar{\kappa}$ is coupled to the number of droplets in the system. The negative values of $\bar{\kappa}$ lead to increase in number of droplets and also the polydispersity. Further, the ratio of saddle-splay modulus to the elastic bending modulus is obtained as $\bar{\kappa}/\kappa \sim -1.3$, which comes in the range $-2 < \bar{\kappa}/\kappa < 0$ as reported for microemulsions [17,21,49,50].

By measuring the shape and size fluctuations of ME droplets using neutron spin echo spectroscopy and small-angle neutron scattering, Farago *et al.* [21] reported $\bar{\kappa}/\kappa \sim -1.89$ for water-AOT-n-decane microemulsions. Further, Würger [50] calculated $\bar{\kappa}/\kappa \sim -2$ for microemulsions from numerical simulations by considering the attractive interaction of hydrophobic tails of surfactant molecules and the entropic contributions. Using ellipsometry and x-ray reflectivity measurements, Meunier and Lee [41] determined the elastic bending constants of AOT surfactant monolayer in MEs and obtained $\bar{\kappa}/\kappa \sim -1.2$. Further, Kellay *et al.* [48] and Binks *et al.* [11] reported negative values of $\bar{\kappa}$ for AOT-brine-oil microemulsions in the droplet phase.

Consequently, it can be inferred that the value of elastic bending constants ($\bar{\kappa}/\kappa$) obtained in the present study compares well with the independent determinations in the literature [21,22,24,41]. Hereby, the proposed method to estimate the saddle-splay modulus of microemulsions using SANS and DRS techniques is validated. This approach can be further verified for the droplet phase of microemulsions with different compositions and also for microemulsions stabilized with other varieties of surfactants.

V. CONCLUSIONS

In conclusion, we have presented a strategy to determine the saddle-splay modulus $\bar{\kappa}$ of interfacial surfactant monolayer in reverse microemulsions from the measured values of effective elastic bending constant K and the elastic bending modulus κ using SANS and DRS techniques. K is determined from the polydispersity of ME droplets, where the thermally influenced droplet deformations are described in terms of spherical harmonics. Further, the temperature-dependent percolation transitions in MEs are monitored and the elastic bending modulus κ is estimated. Notably, the ratio of saddle-splay modulus to the elastic bending modulus is found to be in the range of acceptable limits, $-2 < \bar{\kappa}/\kappa < 0$, reported for the spherical droplet phase of MEs and thus validates the proposed strategy to estimate $\bar{\kappa}$. Further, in the present method, the possibility of precise determination of core radius, polydispersity of droplets, and percolation temperature of microemulsions using SANS and DRS brings out the accessibility to the experimentally elusive saddle-splay modulus of MEs. Finally, the method presented here can be further verified for spherical droplet type microemulsions stabilized with varieties of surfactants.

ACKNOWLEDGMENTS

P.M.G. and D.K.S. acknowledge the financial support from Impacting Research Innovation and Technology (IMPRINT) India initiative, Ministry of Human Resource Development, Government of India, and funding from the UGC-DAE Consortium for scientific research.

[1] M. J. Lawrence and G. D. Rees, Adv. Drug Deliv. Rev. **64**, 175 (2012).
[2] X. Zhao, R. Tapec-Dytioco, and W. Tan, J. Am. Chem. Soc. **125**, 11474 (2003).
[3] B. K. Paul and S. P. Moulik, Curr. Sci. **80**, 990 (2001).
[4] J. Flanagan and H. Singh, Crit. Rev. Food Sci. Nutr. **46**, 221 (2006).
[5] D. O. Shah, *Improved Oil Recovery by Surfactant and Polymer Flooding* (Elsevier, Amsterdam, 2012).
[6] E. J. Acosta, J. H. Harwell, J. F. Scamehorn, and D. A. Sabatini, in *Handbook for Cleaning/Decontamination of Surfaces* (Elsevier, Amsterdam, 2007), pp. 831–884.
[7] P. Boonme, J. Cosmet. Dermatol. **6**, 223 (2007).
[8] D. S. Mathew and R.-S. Juang, Chem. Eng. J. **129**, 51 (2007).
[9] T. Sottmann and C. Stubenrauch, *Microemulsions: Background, New Concepts, Applications, Perspectives* (Wiley Online Library, 2009).
[10] W. Helfrich, Z. Naturforsch., C **28**, 693 (1973).
[11] B. P. Binks, J. Meunier, O. Abillon, and D. Langevin, Langmuir **5**, 415 (1989).
[12] R. Wipf, S. Jaksch, and B. Stühn, Colloid Polym. Sci. **288**, 589 (2010).
[13] P. M. Geethu, I. Yadav, V. K. Aswal, and D. K. Satapathy, Langmuir **33**, 13014 (2017).

[14] E. Van der Linden, S. Geiger, and D. Bedeaux, Physica A (Amsterdam) **156**, 130 (1989).
[15] W. Meier, J. Phys. Chem. B **101**, 919 (1997).
[16] B. Kuttich, P. Falus, I. Grillo, and B. Stühn, J. Chem. Phys. **141**, 084903 (2014).
[17] S. A. Safran, Phys. Rev. A **43**, 2903 (1991).
[18] R. Varadharajan and F. A. M. Leermakers, Phys. Rev. Lett. **120**, 028003 (2018).
[19] H. Bagger-Jörgensen and U. Olsson, Langmuir **12**, 4057 (1996).
[20] M. Hu, J. J. Briguglio, and M. Deserno, Biophys. J. **102**, 1403 (2012).
[21] B. Farago, D. Richter, J. S. Huang, S. A. Safran, and S. T. Milner, Phys. Rev. Lett. **65**, 3348 (1990).
[22] T. Hellweg, M. Gradzielski, B. Farago, and D. Langevin, Colloids Surf. A **183**, 159 (2001).
[23] B. Farago, Physica B (Amsterdam) **226**, 51 (1996).
[24] M. Gradzielski, D. Langevin, and B. Farago, Phys. Rev. E **53**, 3900 (1996).
[25] W. Meier, Langmuir **12**, 1188 (1996).
[26] J. E. Bowcott and J. H. Schulman, Z. Elektrochem. **59**, 283 (1955).
[27] S. T. Milner and S. A. Safran, Phys. Rev. A **36**, 4371 (1987).
[28] S. A. Safran, J. Chem. Phys. **78**, 2073 (1983).
[29] F. Sicoli, D. Langevin, and L. Lee, J. Chem. Phys. **99**, 4759 (1993).
[30] F. Sicoli and D. Langevin, J. Phys. Chem. **99**, 14819 (1995).
[31] P. G. De Gennes and C. Taupin, J. Phys. Chem. **86**, 2294 (1982).
[32] H. Mays and G. Ilgenfritz, J. Chem. Soc. Faraday Trans. **92**, 3145 (1996).
[33] S. A. Safran and L. A. Turkevich, Phys. Rev. Lett. **50**, 1930 (1983).
[34] M. J. Hou and D. O. Shah, Langmuir **3**, 1086 (1987).
[35] S.-H. Chen, Annu. Rev. Phys. Chem. **37**, 351 (1986).
[36] J. S. Pedersen, Adv. Colloid Interface Sci. **70**, 171 (1997).
[37] P. M. Geethu, I. Yadav, S. K. Deshpande, V. K. Aswal, and D. K. Satapathy, Macromolecules **50**, 6518 (2017).
[38] V. K. Aswal and P. S. Goyal, Curr. Sci. **79**, 947 (2000).
[39] I. Breßler, J. Kohlbrecher, and A. F. Thünemann, J. Appl. Crystallogr. **48**, 1587 (2015).
[40] A. Schönhals and F. Kremer, in *Broadband Dielectric Spectroscopy* (Springer, Berlin, 2003), pp. 59–98.
[41] J. Meunier and L. T. Lee, Langmuir **7**, 1855 (1991).
[42] H. T. Jung, B. Coldren, J. A. Zasadzinski, D. J. Iampietro, and E. W. Kaler, Proc. Natl. Acad. Sci. USA **98**, 1353 (2001).
[43] J. N. Israelachvili, D. J. Mitchell, and B. W. Ninham, J. Chem. Soc. Faraday Trans. **72**, 1525 (1976).
[44] D. C. Morse and S. T. Milner, EPL **26**, 565 (1994).
[45] Y. Feldman, N. Kozlovich, I. Nir, and N. Garti, Phys. Rev. E **51**, 478 (1995).
[46] C. Cametti, Phys. Rev. E **81**, 031403 (2010).
[47] M. Nagao, H. Seto, T. Takeda, and Y. Kawabata, J. Chem. Phys. **115**, 10036 (2001).
[48] H. Kellay, B. P. Binks, Y. Hendrikx, L. T. Lee, and J. Meunier, Adv. Colloid Interface Sci. **49**, 85 (1994).
[49] R. H. Templer, B. J. Khoo, and J. M. Seddon, Langmuir **14**, 7427 (1998).
[50] A. Würger, Phys. Rev. Lett. **85**, 337 (2000).